Supporting Information

Stern Model Adsorption of Oligonucleotides on Lamellar Cationic Lipid Bilayer Investigated by Polarization-Resolved SFG-VS

Liqun Wang[1, 2],Yang Shen[1, 3], Yanbo Yang[1, 2], Wangting Lu[1], Wenhui Li[1], Feng Wei[, 1], Guang Zheng[3], Youhua Zhou[3], Wanquan Zheng*[, 1, 4] Yuancheng Cao[5]*

[1] Institution for Interdisciplinary Research, & Key Laboratory of Optoelectronic Chemical Materials and Devices of Ministry of Education, Jianghan University, 430056, Wuhan, Hubei, P. R. China

[2] College of Life Science, Jianghan University, 430056, Wuhan, Hubei P. R. China

[3] School of Physics and Information Engineering, Jianghan University, 430056, Wuhan, Hubei P. R. China

[4] Institut des Sciences Moléculaires d'Orsay, Université Paris-Sud, 91405 Orsay Cedex, France

[5] School of Chemical and Environmental Engineering, Jianghan University, 430056, Wuhan, Hubei, P. R. China

1. SFG-VS spectra in H_2O

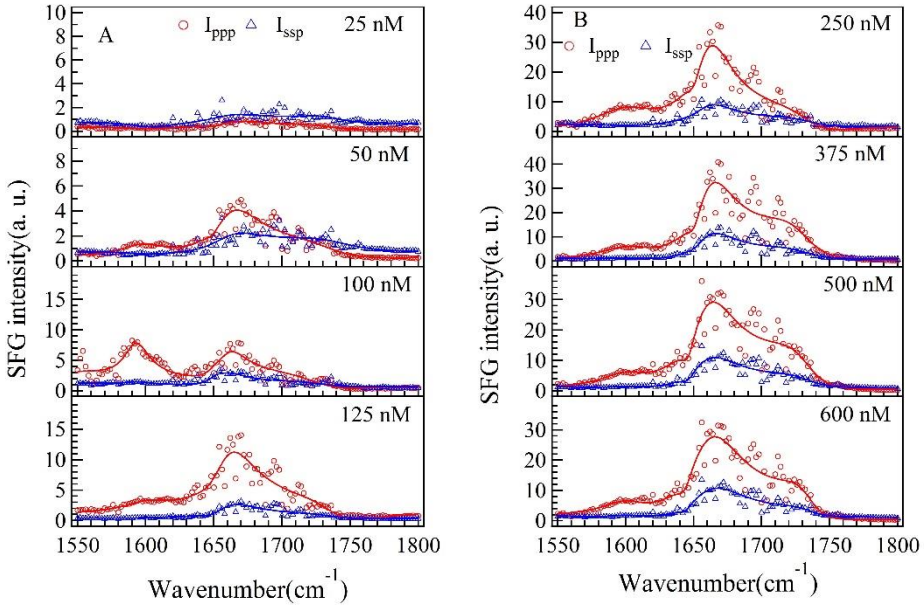

Figure S1 SFG spectra collected in the wavenumber range of 1550-1800 cm^{-1} at various C_{dT}. A. 25 nM – 125 nM. B. 250nM – 600 nM.

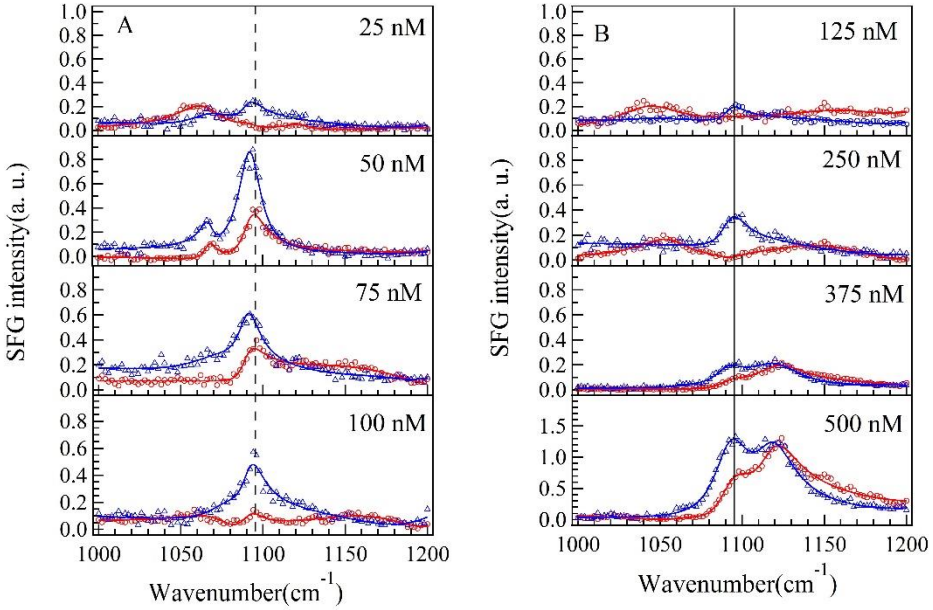

Figure S2 SFG spectra collected in the wavenumber range of 1000-1200 cm^{-1} at various C_{dT}. A. 25 nM – 100 nM. B. 125 nM – 500 nM.

2. SFG-VS spectra in D_2O

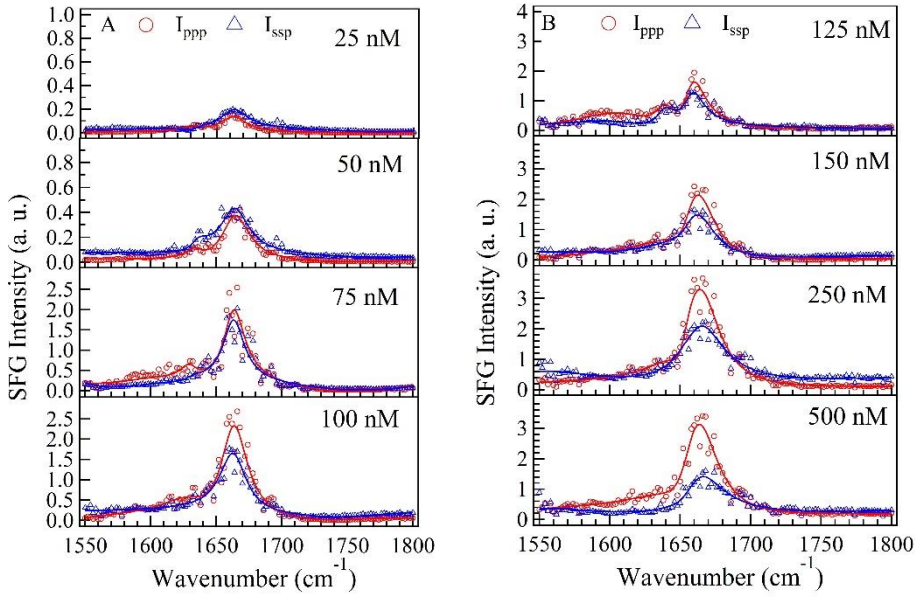

Figure S3 SFG spectra collected in the wavenumber range of 1550-1800 cm^{-1} at various C_{dT}. A. 25 nM – 100 nM. B. 125 nM – 600 nM.

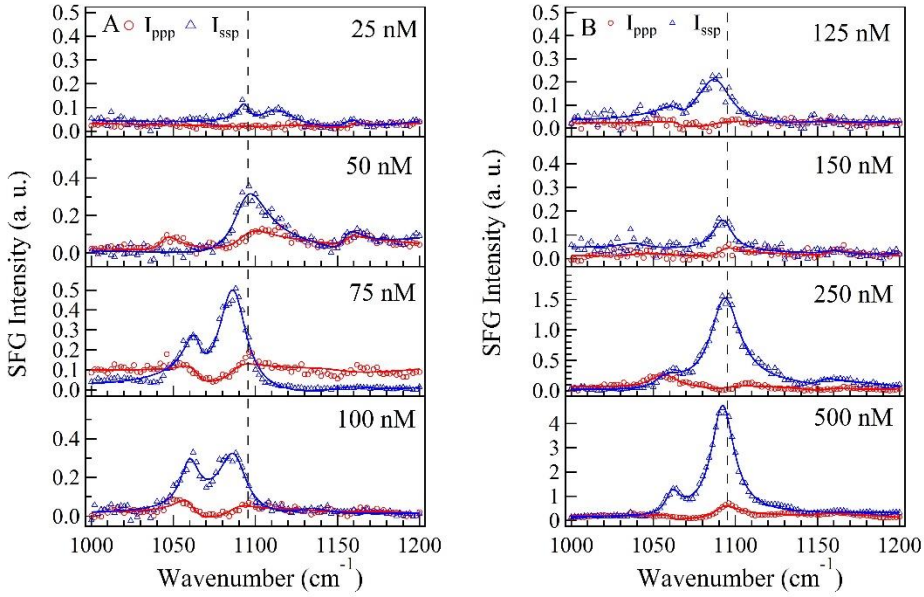

Figure S4 SFG spectra collected in the wavenumber range of 1000-1200 cm^{-1} at various C_{dT}. A. 25 nM – 100 nM. B. 125 nM – 500 nM.

3. Origins of SFG-VS signals at charged surface

Scheme S1 Electronic double layer (EDL) structure of Gouy-Chapmann-Stern model and its contributions to SFG signals

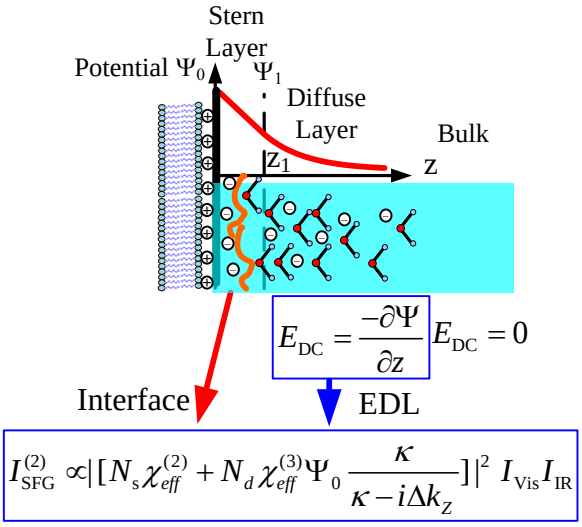

The SFG-VS signals generated from the charged surface have contributions from both the second-order $\chi_{eff}^{(2)}$ and third-order $\chi_{eff}^{(3)}$ nonlinear susceptibilities: [1, 2]

$$I_{SFG} \propto |P^{(2)}|^2 I_{Vis} I_{IR} = |[N_s\chi_{eff}^{(2)} + N_d\chi_{eff}^{(3)}\Psi_0 \frac{\kappa}{\kappa - i\Delta k_Z}]|^2 I_{Vis} I_{IR} \quad (S1)$$

where N_s is the molecular abundance at the interface, N_d is the molecular abundance in the solution of diffusive layer, and Ψ_0 is the surface potential. The sign of Φ_0 is determined by the sum charge density at the surface (σ_{Sum}):

$$\Psi_0 = \frac{2k_BT}{e}\sinh^{-1}\left(\frac{\sigma_{sum}}{8000k_BTN_Ac\varepsilon_0\varepsilon_r}\right) \quad (S2)$$

Thus function S1 indicates that the SFG signals can be generated from both the interfacial adsorbed molecules and the molecules within the electronic double layer. For SFG signals of oligonucleotide molecules, the contribution from $N_d \chi_{eff}^{(3)} \Phi_0 \frac{\kappa}{\kappa - i\Delta k_Z}$ usually can be ignored due to the small concentration (N_d □ N_A*10^{-6}Mol/L) in solution. For SFG signals of H_2O/D_2O molecules ($N_d \approx N_A$*55 Mol/L) at charged lipid bilayer, the contribution from $\chi_{eff}^{(3)}$ can be comparable with the contribution from $\chi_{eff}^{(2)}$. The signs of both terms in function S1 ($N_s \chi_{eff}^{(2)}$ and $N_d \chi_{eff}^{(3)} \Phi_0 \frac{\kappa}{\kappa - i\Delta k_Z}$) are determined by the sign of surface charge ($\sigma_{Sum} = \sigma_{0,DMTAP} + \sigma_{dT_{25}}$). Previous ultrafast vibrational relaxation SFG experimental results and heterodyne SFG-VS results show that water near a charged surface is similar to that of bulk water at ionic strength of 10 mM, which indicate the bulk contribution is the dominant part of function S1 at such concentration.[3-4] When the surface reaches the point of zero charge (PZC), the term of $N_s \chi_{eff}^{(2)}$ is the dominant part of function S1. When the dT_{25} molecules adsorption reaches maximum and the water molecules at the DMTAP/solution interface are excluded by the dT_{25} molecules. $N_{s,D_2O} \approx 0$, the value of SFG intensity is determined solely by $N_d \chi_{eff}^{(3)} \Phi_0 \frac{\kappa}{\kappa - i\Delta k_Z}$.

4. Fitting of SFG-VS Signals

As described in detail elsewhere, the intensity of the SFG light is proportional to the square of the sample's second-order nonlinear susceptibility($\chi_{eff}^{(2)}$), and the intensity of the two input fields $I_1(\omega_{vis})$ and $I_2(\omega_{IR})$, see eq. (S1). $\chi_{eff}^{(2)}$ vanishes when the structure of contributing molecules/medium has an inversion symmetry.[5-11]

$$I(\omega_{SFG}) \propto \left|\chi_{eff}^{(2)}\right|^2 I_1(\omega_{vis}) I_2(\omega_{IR}) \qquad (S3)$$

where $\omega_{SFG} = \omega_{IR} + \omega_{vis}$. As the IR beam frequency is tuned over a vibrational resonance of surface/interface molecules, the effective surface nonlinear susceptibility $\chi_R^{(2)}$ can be greatly enhanced. The frequency dependence of $\chi_{eff}^{(2)}$ is described by eq. (S2)

$$\chi_{eff}^{(2)}(\omega_{SFG}) = \chi_{NR}^{(2)} + \sum_{\upsilon} \frac{A_\upsilon \cdot e^{i\cdot\varphi_\upsilon}}{\omega_{IR} - \omega_\upsilon + i\Gamma_\upsilon} \qquad (S4)$$

Where A_υ, ω_υ, and Γ_υ are the strength, resonant frequency, and damping coefficient of the vibrational mode(ν), respectively. The value of $A_\upsilon \cdot e^{i\cdot\varphi}$ can be either positive or negative depending on the phase φ of the vibrational mode. The plot of SFG signal vs. the IR input frequency shows a polarization-dependent vibrational spectrum of the molecules at surface or interface. A_υ, ω_υ, and Γ_υ can be extracted by fitting the spectrum using eq.S2.

2. Susceptibilities of molecular groups

The molecular orientation information can be obtained by relating SFG susceptibility tensor elements $\chi_{ijk}(i,j,k = x,y,z)$ in the laboratory frame to the SFG molecular hyperpolarizability tensor elements $\beta_{lmn}(l,m,n = a,b,c)$ in the molecular frame via the Euler transformation.[3,4] The Euler transformation used here follows the z-x-y convention, which has a matrix in the form shown in eq.S4.

$$\chi_{ijk,q}^{(2)} = \sum_{l,m,n} N_s \left\langle R_{il} R_{jm} R_{kn} \right\rangle \beta_{lmn,q} \qquad (S5)$$

$$R_{il,\,jm,kn} = \begin{pmatrix} -\sin(\varphi)\cos(\theta)\sin(\psi) + \cos(\varphi)\cos(\psi) & -\sin(\varphi)\cos(\theta)\cos(\psi) - \cos(\varphi)\sin(\psi) & \sin(\varphi)\sin(\theta) \\ \cos(\varphi)\cos(\theta)\sin(\psi) + \sin(\varphi)\cos(\psi) & \cos(\varphi)\cos(\theta)\cos(\psi) - \sin(\varphi)\sin(\psi) & -\cos(\varphi)\sin(\theta) \\ \sin(\theta)\sin(\psi) & \sin(\theta)\cos(\psi) & \cos(\theta) \end{pmatrix} \qquad (S6)$$

The components of $\chi_{eff}^{(2)}$ of ssp, and ppp polarization combinations are given in equations (S5)-(S6) in the lab coordinate system which is defined as the z-axis being along the surface normal and the x-axis being in the incident plane.[5-9]

$$\chi^{(2)}_{eff,ssp} = L_{yy}(\omega_{SF})L_{yy}(\omega_{Vis})L_{zz}(\omega_{IR})\sin\beta_{IR}\chi^{(2)}_{yyz} \quad (S7)$$

$$\begin{aligned}\chi^{(2)}_{eff,ppp} = &-L_{xx}(\omega_{SF})L_{xx}(\omega_{Vis})L_{zz}(\omega_{IR})\cos\beta_{SF}\cos\beta_{Vis}\sin\beta_{IR}\chi^{(2)}_{xxz}\\ &-L_{xx}(\omega_{SF})L_{zz}(\omega_{Vis})L_{xx}(\omega_{IR})\cos\beta_{SF}\sin\beta_{Vis}\cos\beta_{IR}\chi^{(2)}_{xzx}\\ &+L_{zz}(\omega_{SF})L_{xx}(\omega_{Vis})L_{xx}(\omega_{IR})\sin\beta_{SF}\cos\beta_{Vis}\cos\beta_{IR}\chi^{(2)}_{zxx}\\ &+L_{zz}(\omega_{SF})L_{zz}(\omega_{Vis})L_{zz}(\omega_{IR})\sin\beta_{SF}\sin\beta_{Vis}\sin\beta_{IR}\chi^{(2)}_{zzz}\end{aligned} \quad (S8)$$

where β_{SF}, β_{Vis} and β_{IR} are the angles between the surface normal and the sum frequency beam, the input visible beam, and the input IR beam, respectively. L_{ii} (i = x, y or z) denotes the Fresnel coefficients.

2.1 Symmetric PO_2^- stretching:

After considering the Fresnel coefficient constants under this experimental geometry, eqs.(S5-S6) are then given by

$$\chi^{(2)}_{eff,ssp} = 1.100\chi^{(2)}_{yyz} \quad (S9)$$

$$\chi^{(2)}_{eff,ppp} = -0.114\chi^{(2)}_{xxz} + 0.989\chi^{(2)}_{zzz} \quad (S10)$$

The symmetry of PO_2^- group can be treated as C_{2v} symmetry. The peaks at ~ 1090 cm^{-1} can be assigned to A_1 modes.[12] The susceptibility tensor elements of A_1 mode in C_{2v} symmetry are described as following equations.[8-10] A_1 mode:

$$\begin{aligned}\chi^{(2),A1}_{xxz} = \chi^{(2),A1}_{yyz} = &\frac{1}{2}N_s\beta_{ccc}[\langle\cos^2\psi\rangle R_a + \langle\sin^2\psi\rangle R_b + 1]\langle\cos\theta\rangle\\ &+\frac{1}{2}N_s\beta_{ccc}[\langle\sin^2\psi\rangle R_a + \langle\cos^2\psi\rangle R_b - 1]\langle\cos^3\theta\rangle\end{aligned} \quad (S11)$$

$$\begin{aligned}\chi^{(2),A1}_{zzz} = &N_s\beta_{ccc}[\langle\sin^2\psi\rangle R_a + \langle\cos^2\psi\rangle R_b]\langle\cos\theta\rangle\\ &-N_s\beta_{ccc}[\langle\sin^2\psi\rangle R_a + \langle\cos^2\psi\rangle R_b - 1]\langle\cos^3\theta\rangle\end{aligned} \quad (S12)$$

where ψ is the twisting angle of PO_2^- group. Using the bond polarizability derivative model, the polarization ratios of R_a and R_b of $O\cdots P\cdots O$ stretch in dT_{25} molecules is determined by taking $r_{P\text{-}}$

o = 0.2(corresponding Raman depolarization ration is 0.155) and τ=120°.[13]

$$R_a = \frac{\beta_{aac}}{\beta_{ccc}} = \frac{1+r-(1-r)\cos\tau}{1+r+(1-r)\cos\tau} \qquad \text{(S13)}$$

$$R_b = \frac{\beta_{bbc}}{\beta_{ccc}} = \frac{2r}{1+r+(1-r)\cos\tau} \qquad \textit{(S14)}$$

According to eqs.(S16) and (S17), the deduced susceptibility ratio $\chi^{(2)}_{ppp,PO_2^-\text{-}ss} / \chi^{(2)}_{ssp,PO_2^-\text{-}ss}$ at $\psi = 0°$ can be plotted as a function of the tilt angle (shown in Figure S3).

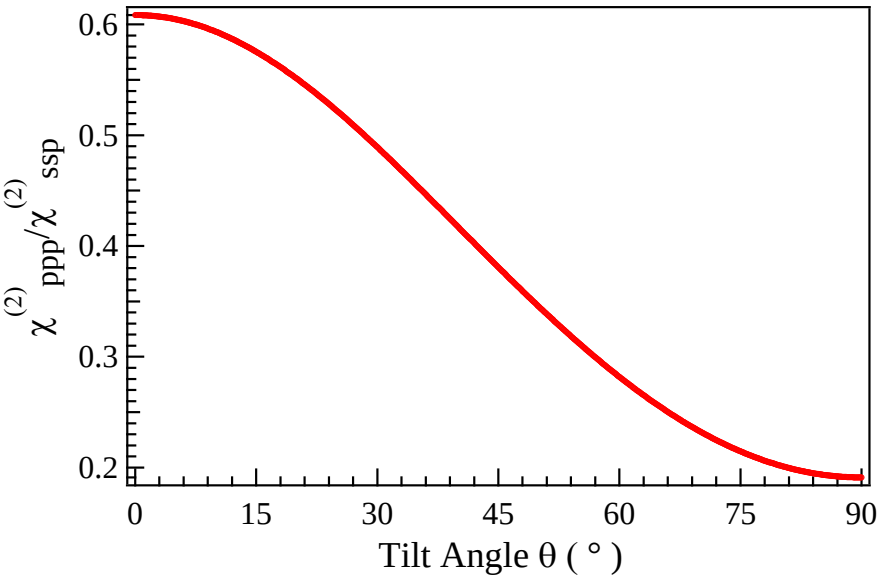

Figure S5 The deduced susceptibility ratio $\chi^{(2)}_{ppp,PO_2^-\text{-}ss} / \chi^{(2)}_{ssp,PO_2^-\text{-}ss}$ is plotted as a function of the tilt angles of PO_2^- group treating $O \cdots P \cdots O$ bond as having C_{2v} symmetry.

2.2 Thymine C_4=O & C_5=C_6 in phase stretching

After considering the Fresnel coefficient constants under this experimental geometry, eqs.(S5-S6) are then given by

$$\chi^{(2)}_{eff,ssp} = 1.319\chi^{(2)}_{yyz} \qquad \textit{(S15)}$$

$$\chi^{(2)}_{\mathrm{eff,ppp}} = -0.137\chi^{(2)}_{\mathrm{xxz}} - 0.110\chi^{(2)}_{\mathrm{xzx}} + 0.105\chi^{(2)}_{\mathrm{zxx}} + 1.184\chi^{(2)}_{\mathrm{zzz}} \quad \textit{(S16)}$$

Because $\chi^{(2)}_{xxz}$ equals to $\chi^{(2)}_{yyz}$ for C_∞ symmetry, the $\chi^{(2)}_{xxz}$ and $\chi^{(2)}_{zzz}$ susceptibility components are the main contributors to the ssp and ppp signals, respectively. With an azimuthal symmetry of the molecules at the interface, the dependence of $\chi^{(2)}_{xxz}$ and $\chi^{(2)}_{zzz}$ susceptibility components on the molecular hyperpolarizability can be described by the following equations. [5-10]

A_1 mode:

$$\begin{aligned}\chi^{(2),A1}_{xxz} = \chi^{(2),A1}_{yyz} = {} & \frac{1}{2}N_s\beta_{ccc}[\langle\cos^2\psi\rangle R_a + \langle\sin^2\psi\rangle R_b + 1]\langle\cos\theta\rangle \\ & + \frac{1}{2}N_s\beta_{ccc}[\langle\sin^2\psi\rangle R_a + \langle\cos^2\psi\rangle R_b - 1]\langle\cos^3\theta\rangle\end{aligned} \quad \textit{(S17)}$$

$$\begin{aligned}\chi^{(2),A1}_{zzz} = {} & N_s\beta_{ccc}[\langle\sin^2\psi\rangle R_a + \langle\cos^2\psi\rangle R_b]\langle\cos\theta\rangle \\ & - N_s\beta_{ccc}[\langle\sin^2\psi\rangle R_a + \langle\cos^2\psi\rangle R_b - 1]\langle\cos^3\theta\rangle\end{aligned} \quad \textit{(S18)}$$

where ψ is the twisting angle of thymine group.

$$R_a = \frac{\beta_{aac}}{\beta_{ccc}} = \frac{\alpha^{(2)}_{aa}}{\alpha^{(2)}_{cc}} \quad \textit{(S19)}$$

$$R_b = \frac{\beta_{bbc}}{\beta_{ccc}} = \frac{\alpha^{(2)}_{bb}}{\alpha^{(2)}_{cc}} \quad \textit{(S20)}$$

According to eqs.(S18) and (S19), the deduced susceptibility ratio $\chi^{(2)}_{\mathrm{ppp,thymine}} / \chi^{(2)}_{\mathrm{ssp,thymine}}$ at $\psi = 0°$ can be plotted as a function of the tilt angle (shown in Figure S3).

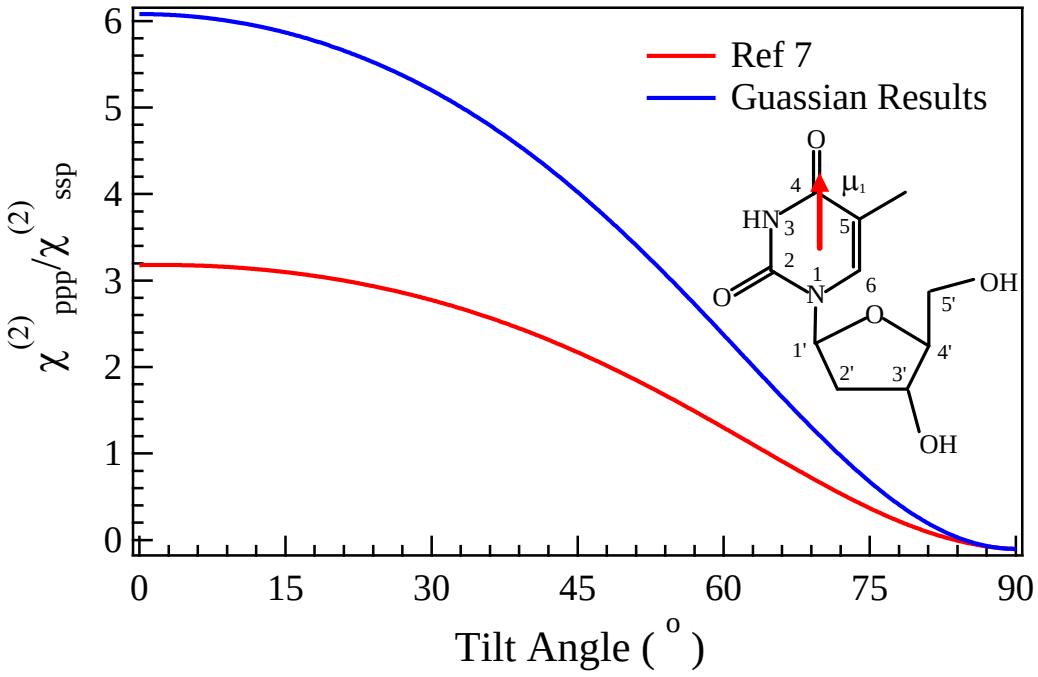

Figure S6 Simulated tile angle dependence of susceptibility ratio $\chi^{(2)}_{ppp}$ / $\chi^{(2)}_{ssp}$ C4=O & C5=C6 in phase stretching of thymine group.

The Raman tensors of thymidine groups at 1660 cm^{-1} has been reported in previous literatures(C1 coordinates, $\frac{\alpha^{(2)}_{aa}}{\alpha^{(2)}_{cc}}$ = 4.31, $\frac{\alpha^{(2)}_{bb}}{\alpha^{(2)}_{cc}}$ = 0.25).[7] The molecular coordinate is determined by taking the plane of thymine aromatic ring as bc plane and taking the $\vec{\mu}_{C_4=O}$ vector as c-axis. The IR dipole moment at wavenumber of C_4=O & C_5=C_6 in phase mode either can be the same as the vector of C_4=O bond or can be calculated using the vibration displacements of each atom ($\frac{\partial x}{\partial Q}, \frac{\partial y}{\partial Q}, \frac{\partial z}{\partial Q}$) listed in the Guassian output file (*.out or *.gjy). [14]

$$\frac{\partial \overrightarrow{\mu_Q}}{\partial Q} = \sum_n M_n \left(\frac{\partial x}{\partial Q}\frac{\partial \mu_n}{\partial x}\vec{x} + \frac{\partial y}{\partial Q}\frac{\partial \mu_n}{\partial y}\vec{y} + \frac{\partial z}{\partial Q}\frac{\partial \mu_n}{\partial z}\vec{z} \right) \qquad (S21)$$

Where M_n is the relative mass of each atom, $\frac{\partial \mu_n}{\partial x}$, $\frac{\partial \mu_n}{\partial y}$ and $\frac{\partial \mu_n}{\partial z}$ are the dipole derivatives of each atom listed at the end of Guassian output file.

Table S1. Derivatives of Raman tensors and IR transition dipoles of C_4=O & C_5=C_6 in phase stretching mode at 1660 cm^{-1}.

Vibrational mode	$\frac{\partial \alpha_{\text{Raman}}}{\partial Q}$	$\frac{\partial \mu_{\text{IR}}}{\partial Q}$	Transformation Matrix
Data from Ref. 7	$\begin{vmatrix} \frac{1}{4.31} & 0 & 0 \\ 0 & \frac{0.25}{4.31} & 0 \\ 0 & 0 & 1 \end{vmatrix}$	$\begin{vmatrix} 0 \\ 0 \\ 1 \end{vmatrix}$	$\begin{vmatrix} 0 & 0 & 1 \\ 0 & 1 & 0 \\ 1 & 0 & 0 \end{vmatrix}$
Calculated Results*	$\begin{vmatrix} 0.329 & 0.137 & -0.283 \\ 0.137 & 0.127 & -0.142 \\ -0.283 & -0.142 & 0.834 \end{vmatrix}$	$\begin{vmatrix} 0 \\ 0 \\ 1 \end{vmatrix}$	$\begin{vmatrix} 0.067 & 0.014 & 0.998 \\ -0.220 & -0.975 & 0.029 \\ 0.973 & -0.222 & -0.062 \end{vmatrix}$

*The derivatives of IR dipole of Thymidine groups was calculated by Guassian 09 using Hartree-fork method with 3-21G+** basis.[14]

Reference

1. Gonella, G.; Lütgebaucks, C.; de Beer, A. G. F.; Roke, S., Second Harmonic and Sum-Frequency Generation from Aqueous Interfaces Is Modulated by Interference. *J. Phys. Chem. C* **2016**, *120*, 9165-9173.
2. Wang, H. F., Sum frequency generation vibrational spectroscopy (SFG-VS) for complex molecular surfaces and interfaces: Spectral lineshape measurement and analysis plus some controversial issues. *Prog. Surf. Sci.* **2016**, *91*, 155-182.
3. Eftekhari-Bafrooei, A.; Borguet, E., Effect of Electric Fields on the Ultrafast Vibrational Relaxation of Water at a Charged Solid–Liquid Interface as Probed by Vibrational Sum Frequency Generation. *J. Phys. Chem. Lett.* 2011, *2*, 1353-1358.

4. Nihonyanagi, S.; Yamaguchi, S.; Tahara, T., Water Hydrogen Bond Structure near Highly Charged Interfaces Is Not Like Ice. *J. Am. Chem. Soc.* **2010,** *132*, 6867-6869**.**

5. Y. R. Shen, The Principles of Nonlinear Optics, 1st ed; John Wiley& Sons: New York, 1984.

6. Moad, A. J.; Simpson, G. J. A Unified Treatment of Selection Rules and Symmetry Relations for Sum-Frequency and Second Harmonic Spectroscopies. *J. Phys. Chem. B* **2004**, *108*, 3548-3562.

7. Chen, X.; Wang, J.; Boughton, A. P.; Kristalyn, C. B.; Chen, Z. Multiple Orientation of Melittin inside a Single Lipid Bilayer Determined by Combined Vibrational Spectroscopic Studies. *J. Am. Chem. Soc.* **2007**, *129*, 1420-1427.

8. Wang, J.; Lee, S. H.; Chen Z. Quantifying the Ordering of Adsorbed Proteins in Situ. *J. Phys. Chem. B* **2008**, *112*, 2281-2290.

9. Nguyen, K. T.; Le Clair, S. V.; Ye, S.; Chen, Z. Orientation Determination of Protein Helical Secondary Structures Using Linear and Nonlinear Vibrational Spectroscopy. *J. Phys. Chem. B* **2009**, *113*, 12169-12180.

10. Lee, S.; Wang, J.; Krimm, S.; Chen, Z. Quantifying the Ordering of Adsorbed Proteins In Situ. *J. Phys. Chem. A* **2006**, *110*, 7035-7044.

11. Thomas, G. J., Jr.; Benevides, J. M.; Overman, S. A.; Ueda, T.; Ushizawa, K.; Saitoh, M.; Tsuboi, M., Polarized Raman spectra of oriented fibers of A DNA and B DNA: anisotropic and isotropic local Raman tensors of base and backbone vibrations. *Biophys. J.* **1995,** *68*, 1073-1088.

12. Benevides, J. M.; Overman, S. A.; Thomas, G. J., Raman, polarized Raman and ultraviolet resonance Raman spectroscopy of nucleic acids and their complexes. *J. Raman Spectrosc.* **2005,** *36*, 279-299.

13. Casillas-Ituarte, N. N.; Chen, X.; Castada, H.; Allen, H. C., Na(+) and Ca(2+) effect on the hydration and orientation of the phosphate group of DPPC at air-water and air-hydrated silica interfaces. *J. Phys. Chem. B* **2010,** *114*, 9485-9495.

14. Gaussian 09, Revision D.01, Frisch, M. J.; Trucks, G. W.; Schlegel, H. B.; Scuseria, G. E.; Robb, M. A.; Cheeseman, J. R.; Scalmani, G.; Barone, V.; Mennucci, B.; Petersson, G. A.; Nakatsuji, H.; Caricato, M.; Li, X.; Hratchian, H. P.; Izmaylov, A. F.; Bloino, J.; Zheng, G.; Sonnenberg, J. L.; Hada, M.; Ehara, M.; Toyota, K.; Fukuda, R.; Hasegawa, J.; Ishida, M.; Nakajima, T.; Honda, Y.; Kitao, O.; Nakai, H.; Vreven, T.; Montgomery, J. A., Jr.; Peralta,

J. E.; Ogliaro, F.; Bearpark, M.; Heyd, J. J.; Brothers, E.; Kudin, K. N.; Staroverov, V. N.; Kobayashi, R.; Normand, J.; Raghavachari, K.; Rendell, A.; Burant, J. C.; Iyengar, S. S.; Tomasi, J.; Cossi, M.; Rega, N.; Millam, M. J.; Klene, M.; Knox, J. E.; Cross, J. B.; Bakken, V.; Adamo, C.; Jaramillo, J.; Gomperts, R.; Stratmann, R. E.; Yazyev, O.; Austin, A. J.; Cammi, R.; Pomelli, C.; Ochterski, J. W.; Martin, R. L.; Morokuma, K.; Zakrzewski, V. G.; Voth, G. A.; Salvador, P.; Dannenberg, J. J.; Dapprich, S.; Daniels, A. D.; Farkas, Ö.; Foresman, J. B.; Ortiz, J. V.; Cioslowski, J.; Fox, D. J. Gaussian, Inc., Wallingford CT, **2009**.